BMC Musculoskeletal Disorders

RESEARCH Open Access

High-fat diet-induced osteoporosis in mice under hypoxic conditions

Yajun Qiao[2,4†], Huimin Zheng[2,3†], Ruiying Cheng[2,4], Juan Guo[1,4,5], Li Ji[1], Zhibin Liu[1], Lixin Wei[2,4], Hongtao Bi[2,4*] and Zhongshu Shan[1*]

Abstract

In the context of global aging, osteoporosis has emerged as a significant public health concern, with a relatively high prevalence observed in plateau regions. This study aimed to investigate the effects and underlying mechanisms of high-fat diet (HFD) and hypoxic conditions on bone metabolism in mice. The mice were subjected to different dietary regimens (a HFD versus a normal diet) and placed in a hypoxic environment. This study explored relevant mechanisms through comprehensive assessments, including body and bone morphological indices, pathological examinations, biochemical analyses, evaluation of gut microbiota diversity, and metabolomics approaches. The results indicated that, compared with those in the control group, the body weight, Lee's index, body mass index (BMI), and body fat percentage of the HFD-fed group were significantly greater. Additionally, the femoral microstructure was compromised, bone metabolic markers were disrupted, inflammatory responses were heightened, gut microbiota diversity was altered, and specific intestinal metabolites such as Anserine were downregulated, whereas L-carnosine was upregulated. Spearman correlation analysis and network visualization elucidated the multifactorial influence mechanism of a HFD on bone metabolism under hypoxic conditions. These factors interconnect to form a complex network that drives osteoporosis development. Notably, L-carnosine occupies a central position within this network, serving as a key hub for interactions among various factors. Under the dual stressors of hypoxia and a HFD, this network becomes imbalanced, leading to bone metabolic disorders and osteoporosis. This study provides insights into the multifactorial mechanisms of osteoporosis induced by a HFD and hypoxia in mice, offering a foundation for subsequent research and preventive strategies for osteoporosis in plateau areas.

Remark

1. This study is not a clinical trial, so there is no clinical trial number. Clinical trial number: not applicable.
2. Western Blot test was not performed in this study, so there were no full uncropped Gels and Blots images (s).

Keywords Hypoxia, HFD, Bone metabolism, Gut

†Yajun Qiao and Huimin Zheng contributed equally to this work.

*Correspondence:
Hongtao Bi
bihongtao@hotmail.com
Zhongshu Shan
zhongshu0320@163.com
[1]Department of Orthopedic Surgery, People's Hospital of Qinghai Province, 2 Gonghe Road, Xining 810007, China
[2]Qinghai Provincial Key Laboratory of Tibetan Medicine Pharmacology and Safety Evaluation, Northwest Institute of Plateau Biology, Chinese Academy of Science, 23 Xinning Road, Xining 810001, China
[3]Department of Pharmacy, Qinghai Minzu University, Xining 810007, China
[4]University of Chinese Academy of Sciences, 19(A) yuquan road, Beijing 10049, China
[5]Xining Chengxi District Center for Disease Control and Prevention, Fuxing Lane 8, Xining 810007, China

Introduction

Osteoporosis is characterized by impaired bone remodeling driven by dysregulated crosstalk between osteoblasts (bone formation) and osteoclasts (bone resorption) [1–2]. Additionally, the high medical costs of osteoporosis impose significant economic burdens on both individuals and governments [3]. Several studies have found that the unique environment at high altitudes exacerbates the occurrence of osteoporosis [4–6]. Hypoxia may be one of the inducing factors for osteoporosis, and the unique hypoxic environment at high altitudes plays a crucial role in bone tissue development [7]. Hypoxia profoundly affects bone metabolism, disrupting the balance between bone formation and resorption to promote osteoporosis [8]. Animal studies have shown that reducing oxygen concentration to 2% inhibits osteoblast mineralization and decreases osteocalcin expression in rats, hindering osteoblast differentiation [9]. Importantly, hypoxia induces a reversible quiescent state in osteoblasts, leading to apoptosis. It impairs mitochondrial respiration by downregulating genes involved in respiration and oxygen consumption rate (OCR) while increasing glycolytic pathway activity [10]. Moreover, hypoxia activates the hypoxia-inducible factor (HIF) signaling pathway. Since osteoclasts rely on glycolysis during bone resorption and HIF enhances glycolysis, hypoxia significantly influences bone metabolism via HIF [11–12]. Additionally, osteoblast-specific activation of HIF-1α promotes osteoclast differentiation [13–14], indicating that HIF plays a central role in mediating communication between osteoblasts and osteoclasts. However, dietary patterns in high-altitude environments differ markedly from those in lowland areas. The plateau diet often involves high intake of protein, calories, and fat [15], with HFD potentially affecting bone metabolism. Most studies show that HFD cause bone loss under normoxic conditions [16–18]; for example, Tencerova et al. found that HFD-induced obesity promotes bone marrow adipose tissue expansion and impairs bone stem cell function in mice [16], while Pickert et al. reported that insulin signaling and Dkk-1 signaling in mice bone marrow may be pathways through which HFD induce bone loss under normoxic conditions [17]. Notably, a few studies in lowland settings suggest HFD may help achieve peak bone mass [19], but this remains inconclusive due to insufficient evidence.

While hypoxia and HFD are each recognized as risk factors for bone loss, their combined impact in high-altitude environments—where chronic hypoxia and increased high-calorie, high-fat food intake coexist—remains poorly understood. Existing evidence suggests these factors may synergistically exacerbate bone loss, such as hypoxia enhancing osteoclastogenesis via HIF-1α-mediated glycolysis and activating pro-inflammatory NF-κB signaling [20–27], and HFD promoting systemic inflammation via gut microbiota dysregulation under normoxic conditions [28–30]. However, most prior studies have investigated hypoxia or HFD in isolation, lacking insights into their potential joint effects on bone metabolism—particularly the mechanisms underlying osteoblast-osteoclast crosstalk under combined exposure, the remote regulatory effects of tissue-specific inflammation in the gut and adipose tissue on bone, and whether HFD-induced gut microbiota dysregulation exacerbates hypoxic stress. Therefore, this study is the first to integrate hypoxic exposure (simulating high-altitude environments) and HFD in a mice model, focusing on inflammatory levels in gut and adipose tissues, as well as changes in gut microbiota and metabolism. The aims are to clarify the skeletal effects of combined exposure, reveal the dual-factor inflammatory network, and fill critical gaps in the pathogenesis of osteoporosis in high-altitude regions, providing a scientific basis for developing preventive strategies targeting "environment-diet" interactions.

Methods

Experimental animals

Forty 5-6-week-old male Kunming (KM) mice were purchased from Sipeifu (Beijing) Biotechnology Co., Ltd. [License number: SCXK (Jing) 2024-0001]. The mice were housed in standard cages with wood chip bedding at a controlled ambient temperature of 22 ± 1 °C under a 12-hour light/dark cycle (artificial lighting from 7:00 AM to 7:00 PM), with free access to standard laboratory diet and distilled water. All animal procedures complied with the ARRIVE guidelines and the National Institutes of Health Guidelines for the Care and Use of Laboratory Animals (NIH Publication No. 8023, revised 1978), and were approved by the Animal Ethics Committee of the Northwest Plateau Biology Institute, Chinese Academy of Sciences (License number: NWIPB20171106-01). During the experiment, cervical dislocation was employed as the euthanasia method for each mice.

Test grouping and treatment

Mice were first fed a high-fat diet (60 kcal% fat; Item number: D12492) for two weeks to induce obesity susceptibility. After weighing, 16 mice with the highest body weights (indicating obesity-prone phenotypes) were selected. To ensure baseline comparability, these mice were then randomly assigned to the control group ($n = 8$) and HFD group ($n = 8$) using a computer-generated random number table (GraphPad Prism 9). Prior to grouping, body weights were compared between groups via independent t-test to confirm no significant differences ($p > 0.05$). Both groups were housed in a hypoxic incubator (oxygen concentration: 16%, simulating 2000–2200 m altitude) [31]. The control group received a standard

laboratory diet, while the HFD group continued on the high-fat diet for an additional 8 weeks. Body weights were recorded weekly, and the experimental procedure is illustrated in Fig. 1 [32].

Measurement of body weight, body length, body fat percentage, Lee's index, and BMI

After the behavioral tests, the mice were deprived of water for 12 h. The following day, their final body weight and length were measured. The Lee index and BMI coefficients were subsequently calculated. The mice were then anesthetized with isoflurane, and the wet weights of the subcutaneous fat in the groin, epididymal fat, perirenal fat, and brown fat in the scapular region were recorded. Body fat percentage, Lee's index, and BMI were computed according to the formulas detailed in Table 1.

Micro-CT detection of mice femurs

Mice were humanely euthanized, and left femurs were isolated, with attached tissues removed. Samples were fixed in 4% paraformaldehyde for 24 h, blotted dry, and scanned using a micro-CT device. Scanning parameters were optimized for femur characteristics: tube voltage 60 kV, current 200 μA, layer thickness 0.2 mm, covering the distal femur. Data were acquired at 0.6° steps over 180° using SkyScan software, reconstructed with NRecon, and postprocessed in Data Viewer. Three-dimensional images were analyzed for regions of interest: cancellous bone (1–1.7 mm below the epiphysis) and cortical bone (2.3–3 mm below the epiphysis). Calculated indices included bone volume fraction (BV/TV), trabecular separation (Tb.Sp), thickness (Tb.Th), number (Tb.N), cortical thickness (Ct.Th), and total void volume (BV). Results were recorded by sample ID for statistical analysis [35].

Pathological analysis of bone, gut, and adipose tissue

After 8 weeks of HFD, mice were euthanized, and colon, inguinal, and epididymal adipose tissues were promptly excised on ice. Femurs were decalcified in 10% EDTA for 1–3 weeks (solution changed every 2–3 days) post-micro-CT [36]. Tissues were fixed in 4% paraformaldehyde, paraffin-embedded, and sectioned at 5 μm. HE staining was performed on colon and adipose tissue sections for pathological evaluation using a light microscope. For bone tissue, 3–5 μm sections were dewaxed, rehydrated, and treated with 3% H_2O_2 to inactivate peroxidase. After PBS washes, sections were stained with TRAP solution at 37 °C for 30–60 min, counterstained with hematoxylin, differentiated, dehydrated, cleared, and mounted for microscopy [37].

Quantification of monoamine neurotransmitters, Hypoxia-Inducible factors, immune factors, and indices of gut injury via Enzyme-Linked immunosorbent assays (ELISAs)

After behavioral tests, mice were anesthetized with isoflurane. Blood was collected via cardiac puncture into anticoagulant-containing tubes, mixed gently, and plasma was isolated by centrifugation at 4 °C, 3000 rpm for 5 min. Mice were euthanized, and colon, inguinal, and epididymal tissues were harvested and stored in PBS (pH 7.4). Tissues were homogenized at 60 Hz, 1800 rpm for 2 min, then centrifuged at 4 °C, 5000 rpm for 10 min to obtain supernatants. Plasma and tissue samples were stored at -80 °C. Levels of alkaline phosphatase (ALP), parathyroid hormone (PTH), vitamin D (VD), HIF-1α, HIF-2α, TNFα, IL-4, IL-6, IL-10, calprotectin (CALP) and lipopolysaccharide (LPS) were quantified by ELISA following the manufacturer's instructions using an EnSpire 2300 plate reader at 450 nm. ELISA kits were from Quanzhou Jiubang Biotechnology Co., Ltd., China.

16 S rDNA analysis

To assess gut microbiota changes, fresh rectal contents were collected from isoflurane-anesthetized mice, frozen in liquid nitrogen, and stored at − 80 °C. DNA was extracted from samples ($n = 6$ per group) using the Mag-Bind Soil DNA Kit, with purity/concentration evaluated by 1% agarose gel electrophoresis. The V3–V4 hypervariable region of 16 S rDNA was amplified via PCR using primers 338 F/806R. Amplicons were purified and sequenced on the Illumina NovaSeq 600 platform. Paired-end reads were merged by FLASH, and OTU clustering/species annotation were performed using UPARSE. Bacterial relative abundances (phylum to species level) were visualized via Krona charts [38].

Metabolite analysis

Metabolomics analyzed gut differential metabolites. After 16 S rDNA sequencing, samples were analyzed by UHPLC coupled with quadrupole time-of-flight mass spectrometry. A BEH Amide column (2.1 mm × 100 mm, 1.7 μm) was used for HILIC separation with mobile phases: A (25 mM ammonium acetate/ammonium hydroxide in water), B (acetonitrile). The gradient was: 95% B (0.5 min) → 65% B (6.5 min) → 40% B (1 min) → 95% B (0.1 min), with 3 min re-equilibration. ESI source conditions: Gas1/Gas2 at 60 °C, CUR 30 °C, source temp 600 °C, ISVF ± 5500 V. MS scans covered m/z 60–1000 (0.20 s/spectrum); auto MS/MS scanned m/z 25–1000 (0.05 s/spectrum) with CE 35 V ± 15 eV. Raw data were converted to MzXML and processed with XCMS for peak grouping, retention time correction and peak area extraction [39].

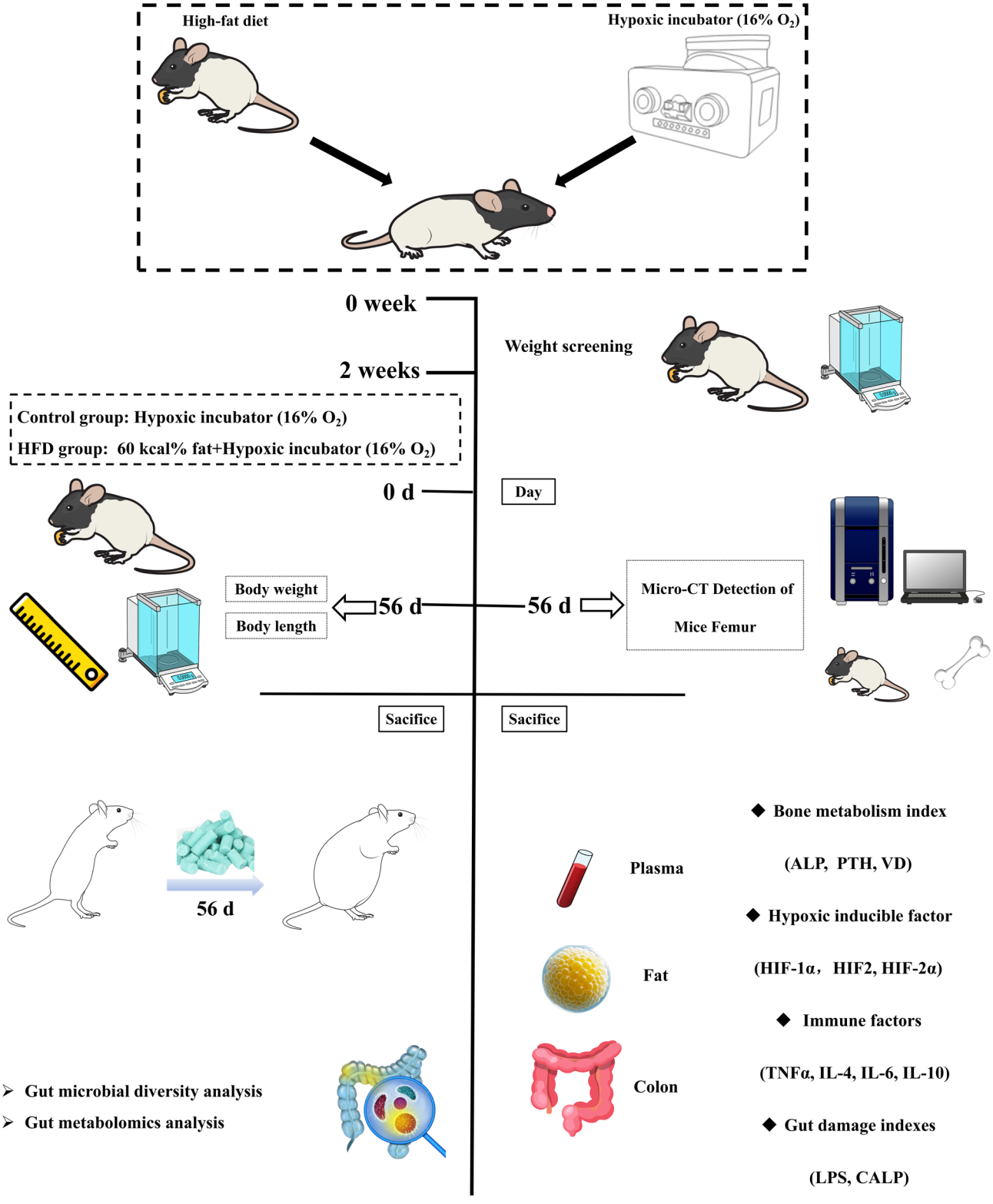

Fig. 1 Testing flowchart

Table 1 Formulas for calculating body fat percentage, Lee's index, and BMI [33–34]

Body fat percentage	[groin fat + epididymal fat + perirenal fat + brown fat] (g)/body weight (g) × 100%
Lee's index	Body weight $^{1/3}$ (g)/Body length (cm) × 1000
BMI	Body weight (g)/Body length ^{2} (cm)

Statistical methods

All the data are presented as the means ± standard deviations (SDs). The samples in the two groups were generally normally distributed. A fully randomized experimental design was employed, and independent sample t tests were conducted via SPSS 22.0 software to compare the mean values between groups. Levene's test was used to assess homogeneity of variance. In cases where variances were unequal, Welch's t test was applied for correction. Spearman correlation analysis was also performed via SPSS 22.0. A p value < 0.05 was considered statistically significant. Data visualization was carried out via Origin 2022 software.

Results

Effects of HFD on body weight, Lee's index, BMI, and body fat percentage in mice under hypoxic conditions

As shown in Fig. 2A1, the body weights of the mice in the HFD group significantly increased over time compared with those of the control group (7 days: 15.09%, $P < 0.001$; 14 days: 6.73%, $P < 0.001$; 21 days: 21.46%, $P < 0.001$; 28 days: 29.65%, $P < 0.001$; 35 days: 32.63%, $P < 0.001$; 42 days: 28.85%, $P < 0.001$; 49 days: 29.35%, $P < 0.001$; 56 days: 15.83%, $P < 0.001$). In the intragroup comparisons (Fig. 2A2), the body weights of the mice in the control group also increased significantly over time (7 days: 4.21%; 14 days: 20.03%, $P < 0.001$; 21 days: 25.14%, $P < 0.001$; 28 days: 25.05%, $P < 0.001$; 35 days: 30.45%, $P < 0.001$; 42 days: 36.19%, $P < 0.001$; 49 days: 37.62%, $P < 0.001$; 56 days: 48.61%, $P < 0.001$). However, the rate of increase was markedly more pronounced in the HFD group (7 days: 20.22%, $P < 0.001$; 14 days: 28.41%, $P < 0.001$; 21 days: 52.36%, $P < 0.001$; 28 days: 62.52%, $P < 0.001$; 35 days: 73.43%, $P < 0.001$; 42 days: 75.90%, $P < 0.001$; 49 days: 78.44%, $P < 0.001$; 56 days: 72.54%, $P < 0.001$).

Specifically, the body weight of the mice in the HFD group was approximately 1.22 times greater than that of the control group at various time points (7 days: 1.15; 14 days: 1.07; 21 days: 1.21; 28 days: 1.30; 35 days: 1.33; 42 days: 1.29; 49 days: 1.29; 56 days: 1.16), with the most substantial difference observed at 35 days. As shown in Fig. 2B and C, after 56 days of HFD consumption, the Lee index (7.12%, $P < 0.01$), BMI (22.20%, $P < 0.01$), and body fat percentage (109.32%, $P < 0.01$) of the mice in the HFD group were significantly greater than those in the control group.

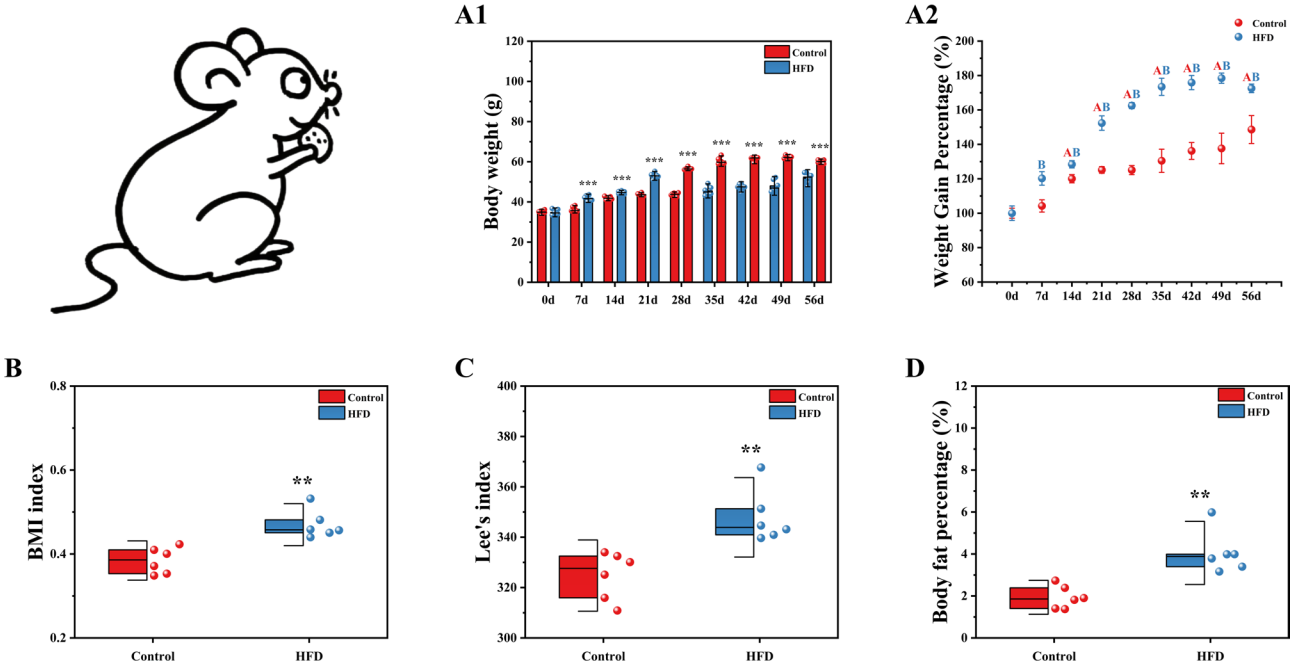

Fig. 2 Effects of a HFD on (**A**) body weight, (**B**) Lee's index, (**C**) body mass index (BMI), and (**D**) body fat percentage in hypoxic mice.Note: Data are expressed as the means ± SDs ($n = 6$). $^{**}P < 0.01$ and $^{***}P < 0.001$ indicate significant differences versus the control group. Comparisons of body weight gain rates at different time points: A denotes a significant difference ($P < 0.001$) between the day 0 group and the control group; B indicates a significant difference ($P < 0.001$) compared with the HFD group on day 0

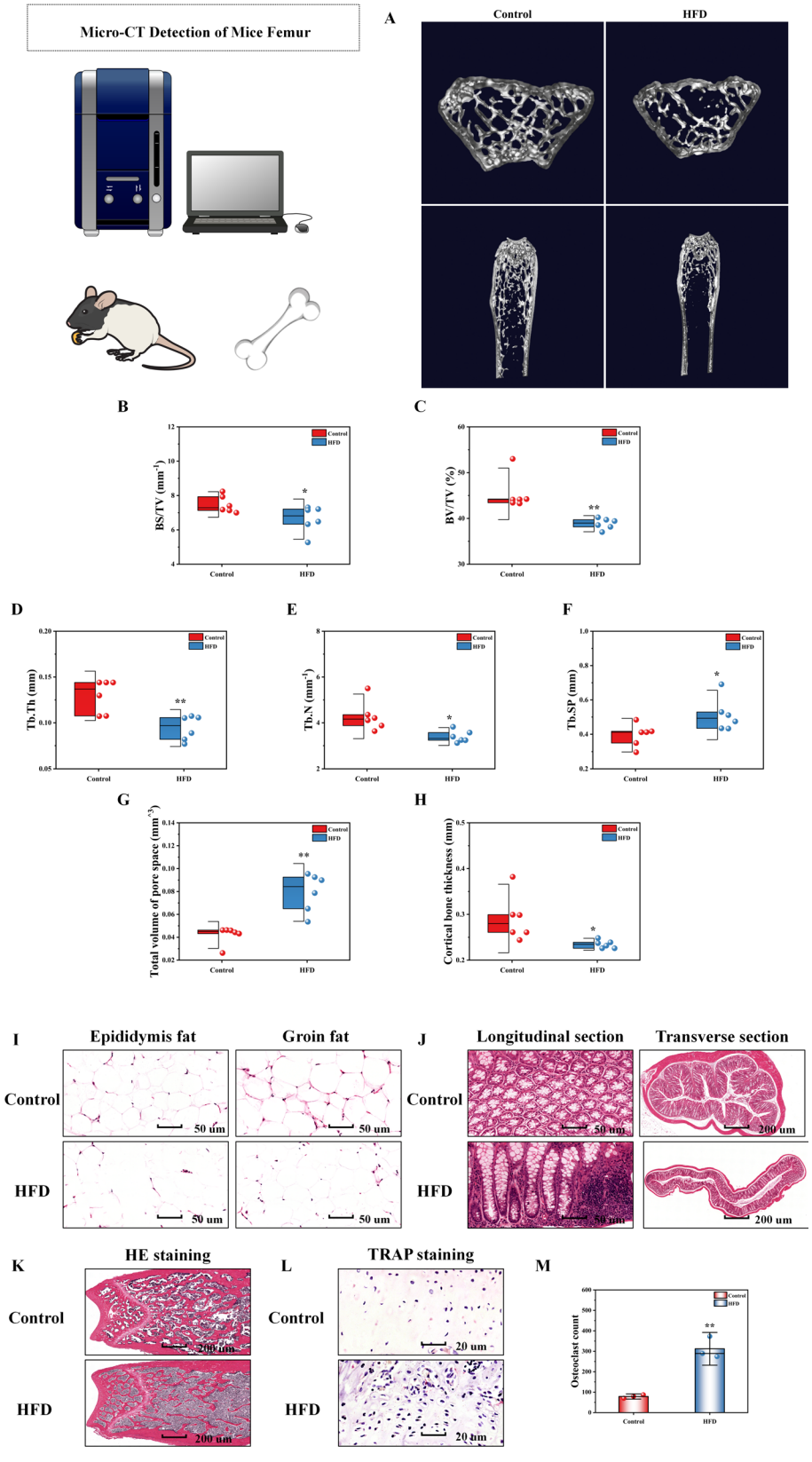

Fig. 3 (See legend on next page.)

(See figure on previous page.)

Fig. 3 The effects of a HFD on the femurs, colon, and adipose tissue of mice under hypoxic conditions. Note: (**A**) Micro-CT scan image of femur; (**B**) bone volume to tissue volume ratio (BV/TV, %); (**C**) bone surface to tissue volume ratio (BS/TV, mm^{-1}); (**D**) trabecular number (Tb.N, mm^{-1}); (**E**) trabecular spacing (Tb.Sp, mm); (**F**) trabecular thickness (Tb.Th, mm); (**G**) cortical thickness (Ct.Th, mm); (**H**) pore volume (Po.V, mm^3); (**I**) HE staining of adipose tissue (scale bar = 40 μm); (J) HE staining of colon tissue (longitudinal section: scale bar = 40 μm; cross section: scale bar = 200 μm); (**K**) HE staining of femur tissue (scale bar = 200 μm); (**L**) TRAP staining of femur tissue (scale bar = 20 μm); (**M**) Number of osteoclasts in femoral tissue.The data are presented as the means ± SDs (**A**-**H**: $n = 6$; **I**-**M**: $n = 3$). *$P < 0.05$ and **$P < 0.01$ indicate statistically significant differences compared with the control group

Micro-CT was utilized to examine the impact of a HFD on the femoral architecture of mice under hypoxic conditions

As illustrated in Fig. 3A, compared with the control group, the HFD group exhibited partial disruption of the femoral trabecular network in cross-sectional images and a markedly sparser porous structure in longitudinal sections. As shown in Fig. 3B-H, compared with those in the control group, significant reductions in BV/TV (14.36%, $P < 0.01$), BS/TV (11.43%, $P < 0.05$), Tb.N (20.62%, $P < 0.01$), Tb.Th (27.12%, $P < 0.01$), and Ct.Th (19.33%, $P < 0.05$) were detected. Conversely, there were significant increases in Tb.Sp (29.65%, $P < 0.05$) and Po.V (88.31%, $P < 0.01$).

Effects of HFD on femur, colon, and adipose tissues in mice under hypoxic conditions

HE staining of adipose tissue (Fig. 3I) revealed that, compared with those in the control group, epididymal and inguinal fat cells in the HFD group were significantly enlarged. The number of intracellular lipid droplets increased, and they fused, leading to an expanded cellular appearance, reduced intercellular space, and denser cell distribution. HE staining of colon tissue (Fig. 3J) revealed that, relative to those in the control group, the intestinal epithelial cells in the HFD group exhibited a disordered arrangement and partial shedding of cells. Additionally, there was increased infiltration of immune cells in the lamina propria, decreased length and density of the intestinal villi, an irregular villus shape, and some instances of villus atrophy, shortening, or even rupture.

HE staining of femur tissue (Fig. 3K) revealed that the bone trabecular structure in the control group was dense and uniform, with complete and clear connections between trabeculae. In contrast, the HFD group presented sparse trabecular bone, thinner trabeculae, and wider spacing between trabeculae. Moreover, the number of hematopoietic cells in the bone marrow cavity of HFD-fed mice was significantly reduced, whereas the number of fat cells increased. Tartrate-resistant acid phosphatase (TRAP) staining (Fig. 3L) indicated that the osteoclast distribution in the femur tissue of control mice was relatively sparse and dispersed. In the HFD group, not only did the number of osteoclasts increase, but their distribution also became more concentrated. Furthermore, the number of osteoclasts in the HFD group was significantly greater than that in the control group (Fig. 3M, $P < 0.01$).

Effects of HFD on bone metabolism indices in the plasma, adipose tissue, and Colon of mice under hypoxic conditions

As illustrated in Fig. 4A, compared with those in the control group, the plasma ALP level in the HFD group significantly increased by 54.66% ($P < 0.001$) and the PTH level significantly decreased by 46.19% ($P < 0.001$), whereas the VD level significantly decreased by 9.38% ($P < 0.001$). Figure 4B shows that, relative to those in the control group, the ALP and PTH levels in the groin fat of the HFD group significantly increased by 21.84% ($P < 0.001$) and 231.09% ($P < 0.001$), respectively, whereas the VD level significantly decreased by 8.57% ($P < 0.01$). As depicted in Fig. 4C, compared with those in the control group, the levels of PTH in the colon tissue of the HFD group were significantly greater (141.09%, $P < 0.001$), whereas the ALP and VD levels were significantly lower (15.33%, $P < 0.01$) and 7.17%, $P < 0.01$), respectively. Figure 4D shows that, compared with those in the control group, the ALP, PTH, and VD levels in the colon were significantly greater in the HFD group (36.52% [$P < 0.01$], 37.16% [$P < 0.01$], and 10.16% [$P < 0.01$], respectively).

Effects of a HFD on gut damage and Hypoxia-Inducible factor indices in the Colon of mice under hypoxic conditions

As shown in Fig. 5A, compared with those in the control group, CALP levels were significantly increased by 15.20% ($P < 0.01$), and LPS levels were significantly increased by 33.83% ($P < 0.001$). As depicted in Fig. 5B, compared with those in the control group, the HIF-1α level increased by 41.07% ($P < 0.001$), the HIF-2 level increased by 62.30% ($P < 0.001$), and the HIF-2α level increased by 66.21% ($P < 0.001$).

Effects of HFD on inflammatory responses in mice under hypoxic conditions

As shown in Fig. 5C, compared with the control group, the HFD group presented a significant increase in plasma TNFα levels (44.94%, $P < 0.01$) and in IL-6 levels (13.57%, $P < 0.001$), whereas the IL-10 level decreased by 5.92%, $P < 0.05$). As shown in Fig. 5D, relative to the control group, the HFD group presented a 73.69% increase in TNFα levels ($P < 0.01$) and a 56.13% increase in IL-6 levels ($P < 0.001$) within groin fat, with IL-10 levels decreasing by 17.19% ($P < 0.01$). As shown in Fig. 5E, compared with those from the control group, epididymal fat from

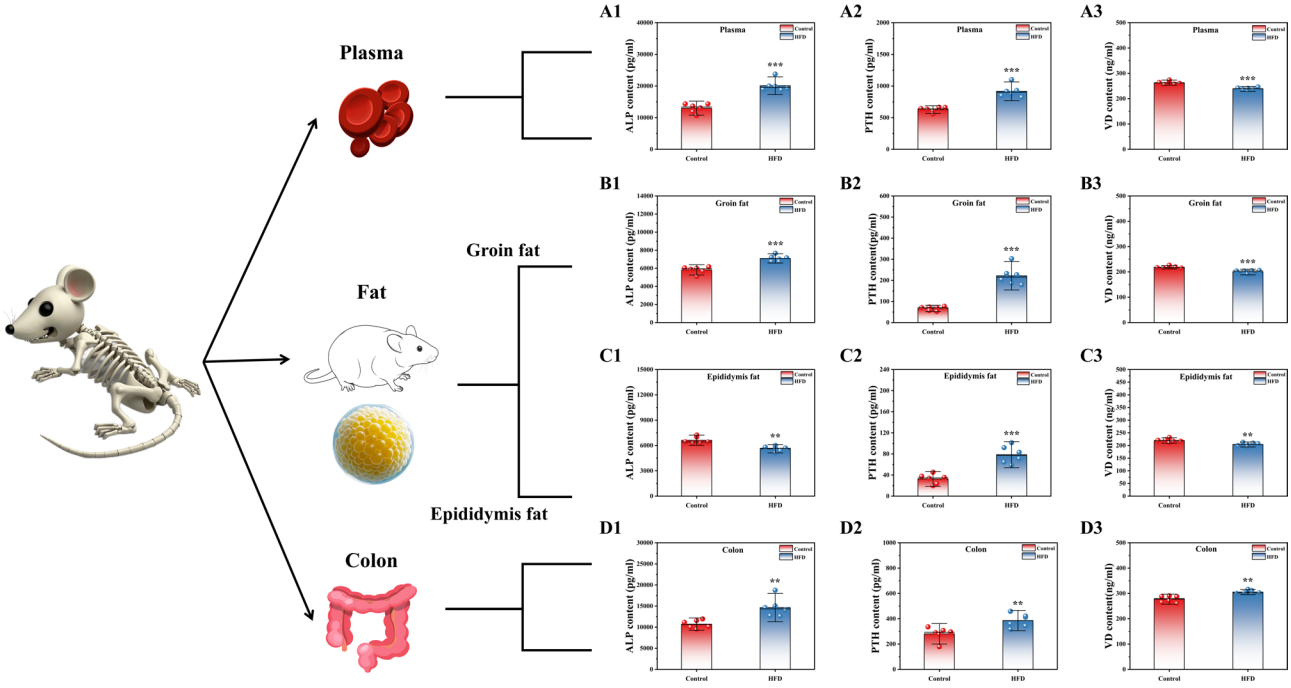

Fig. 4 Effects of a HFD on bone metabolism indices in the plasma, adipose tissue and colon of mice under hypoxia. Note: (**A**) Plasma levels of bone metabolism indicators; (**B**) levels of bone metabolism markers in groin fat; (**C**) levels of bone metabolism markers in epididymal fat; (**D**) levels of bone metabolism indicators in the colon. The data are shown as the means ± SDs ($n = 6$). $^{**}P < 0.01$ and $^{***}P < 0.001$ indicate a significant difference from the control group

the HFD group presented a 23.49% increase in TNFα levels ($P < 0.01$), a 56.62% increase in IL-6 levels ($P < 0.01$), and a 32.86% decrease in IL-10 levels ($P < 0.001$). Finally, as depicted in Fig. 5F, the HFD group experienced a substantial increase in TNFα levels of 262.54% ($P < 0.001$) and in IL-6 levels of 50.35% ($P < 0.001$), along with a 24.42% reduction in IL-10 levels ($P < 0.01$).

Effects of HFD on gut microbiota diversity in mice under hypoxic conditions

Alpha and beta diversity analysis of the gut microbiota

In the alpha diversity analysis (Fig. 6A), compared with the control group, the HFD group presented statistically significant reductions in ACE (abundance-based coverage estimator, $P < 0.001$), Chao1 ($P < 0.001$), and Shannon ($P < 0.001$) indices and an increase in the Simpson index ($P < 0.01$). These results indicate a decrease in species richness and evenness within the HFD group. Principal coordinate analysis (PCoA) based on the Bray–Curtis distance (Fig. 6B) revealed distinct clustering patterns in microbiota composition and structure between the control and HFD groups, as evidenced by PC1 (41.3%), PC2 (32.1%), and PC3 (11.5%). These findings suggest that a HFD significantly alters the overall microbial community structure under hypoxic conditions.

LEfSe (linear discriminant analysis effect size) analysis is illustrated in Fig. 6C. The cladogram depicts the genus-level microbial taxa that significantly contribute to group differentiation. According to the statistical analysis, genera such as *Bacteroides*, *Rikenellaceae RC9 gut group*, *uncultured taxa*, *Helicobacter*, *Mucispirillum*, *Anaeroplasma*, *Dubosiella*, *Faecalibaculum*, *Lactobacillus*, *Lactococcus*, *Anaerofustis*, *Anaerostipes*, *Lachnoclostridium*, *Lachnospiraceae UCG-006*, *Monoglobus*, *UCG-005*, *Paludicola*, *Eubacterium siraeum group*, *UCG-010*, *Eubacterium coprostanoligenes group*, *Family XI UCG-001*, *Parasutterella*, *Psychrobacter*, and *Akkermansia* were identified as important subgroups of the gut microbiota in the control group. In contrast, *Muribaculaceae*, *Muribaculum*, *Prevotellaceae UCG-001*, *uncultured taxa*, *Erysipelatoclostridiaceae*, *Enterococcus*, *Vagococcus*, *Staphylococcus*, *Tuzzerella*, *Colidexribacter*, *Anaerotruncus*, *Anaerovorax*, *Sneathia*, and *Escherichia-Shigella* were significantly different microflora in the HFD group. Additionally, the histogram of the LDA value distribution (Fig. 6C2) highlights species with an LDA score greater than the threshold of 3, indicating statistically significant differences between groups. Specifically, 14 species in the control group and 10 species in the model group exhibited notable differences.

KEGG functional prediction of the gut microbiota

The KEGG functional prediction of the gut microbiota is illustrated in Fig. 6D. At the third hierarchical level, the differential pathways identified included glycolysis/gluconeogenesis; pyruvate metabolism; cysteine and

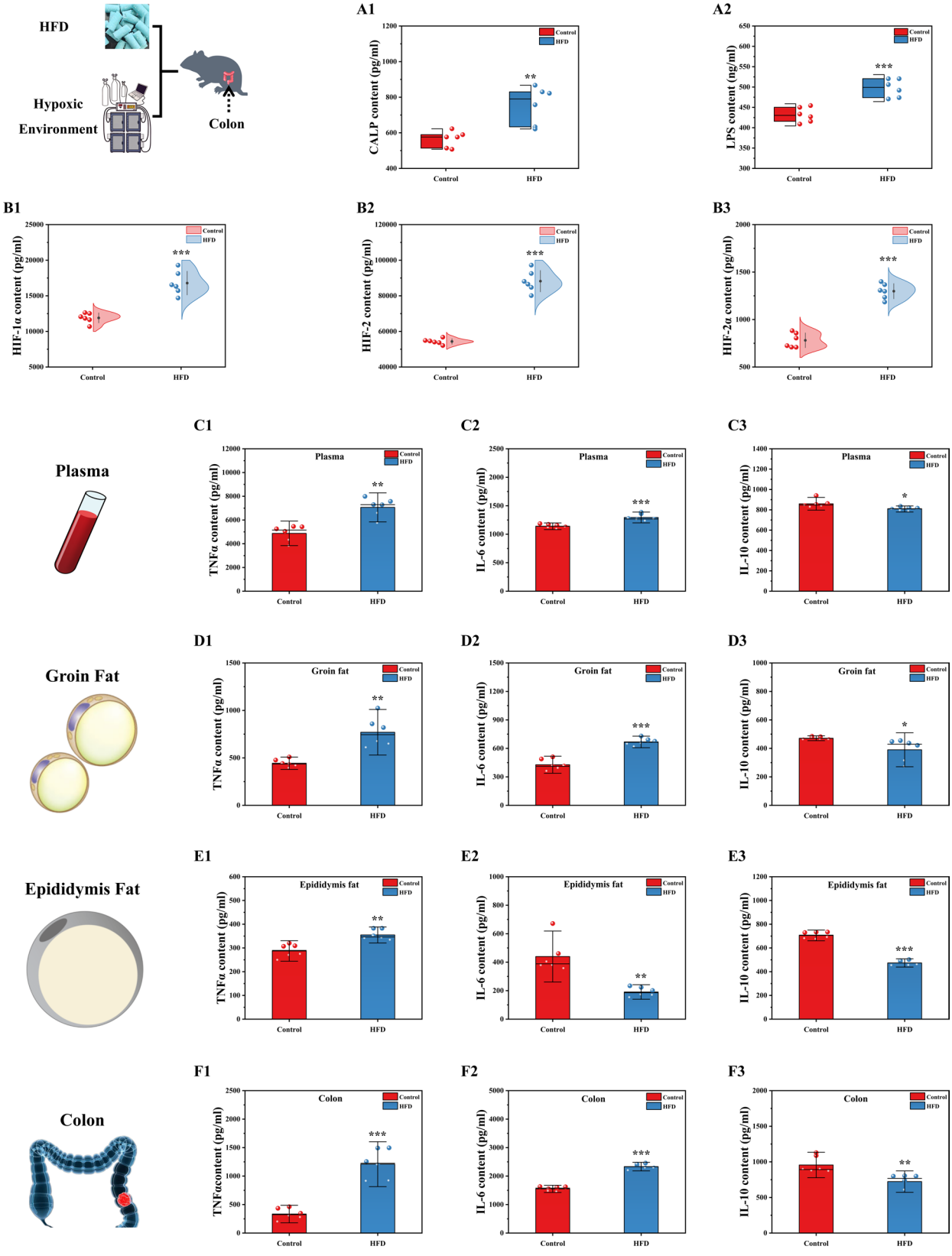

Fig. 5 HFD-induced gut injury and cytokine levels in plasma, adipose tissue, and colon of mice under hypoxic conditions. Note: (**A**) Gut damage indices; (**B**) Colons HIF indices; (**C**) Plasma cytokine levels; (**D**) Groin fat cytokine levels; (**E**) Epididymal fat cytokine levels; (**F**) Colon cytokine levels. The data are presented as the means ± SDs ($n = 6$). *$P < 0.05$, **$P < 0.01$, and ***$P < 0.001$ indicate statistically significant differences compared with the control group

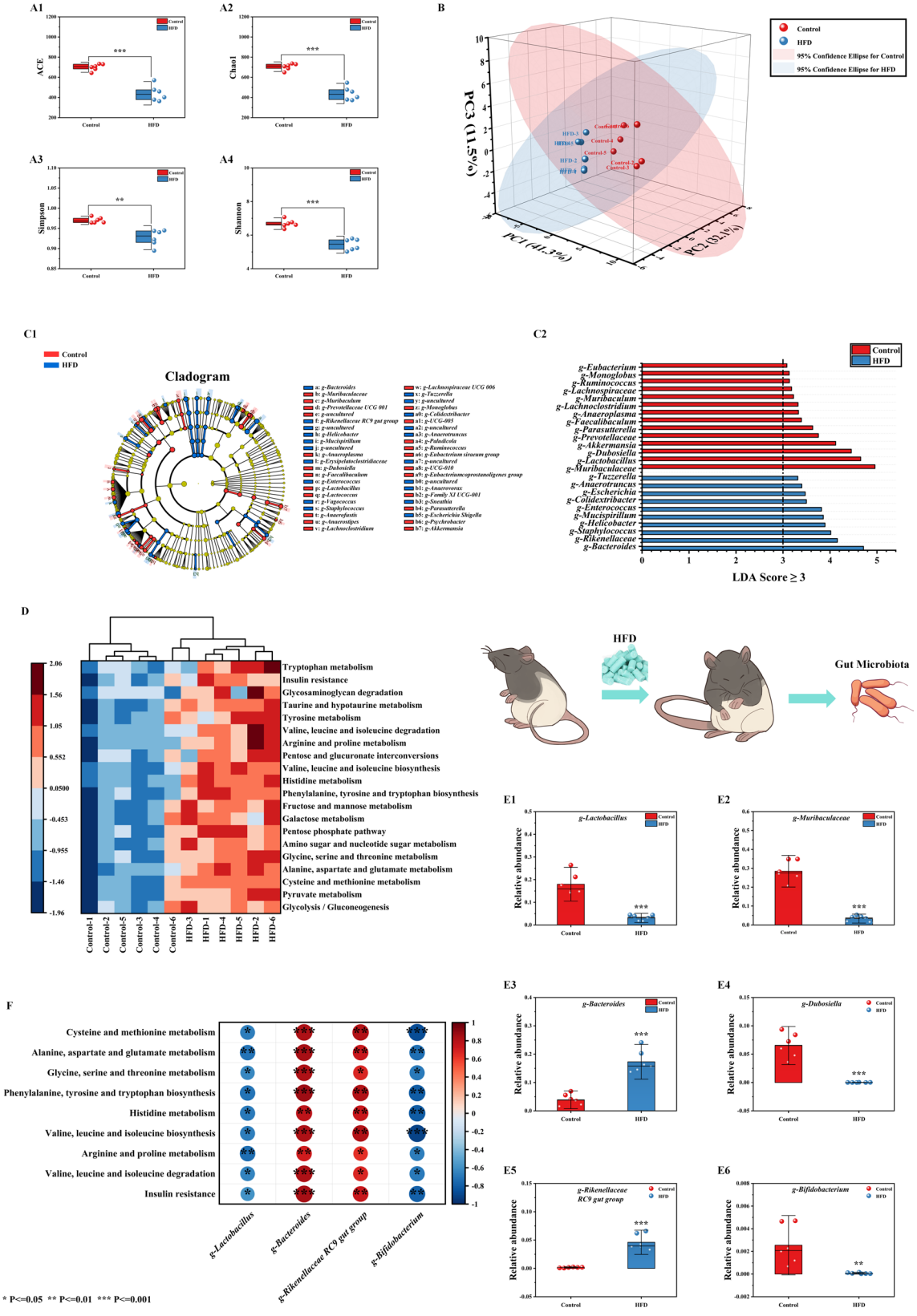

Fig. 6 Impact of HFD on Gut Microbiota Diversity in Mice Under Hypoxic Conditions. Notes: (**A**) α-Diversity analysis; (**B**) β-diversity analysis; (**C**) LEfSe analysis; (**D**) KEGG pathway function prediction at level L3; (**E**) genus -level composition analysis of differentially abundant gut microbiota; (**F**) Correlation analysis between functional pathways and differentially abundant gut microbiota. The data are presented as the means ± SDs ($n = 6$). $^{**}P < 0.01$ and $^{***}P < 0.001$ indicate statistically significant differences relative to the control group

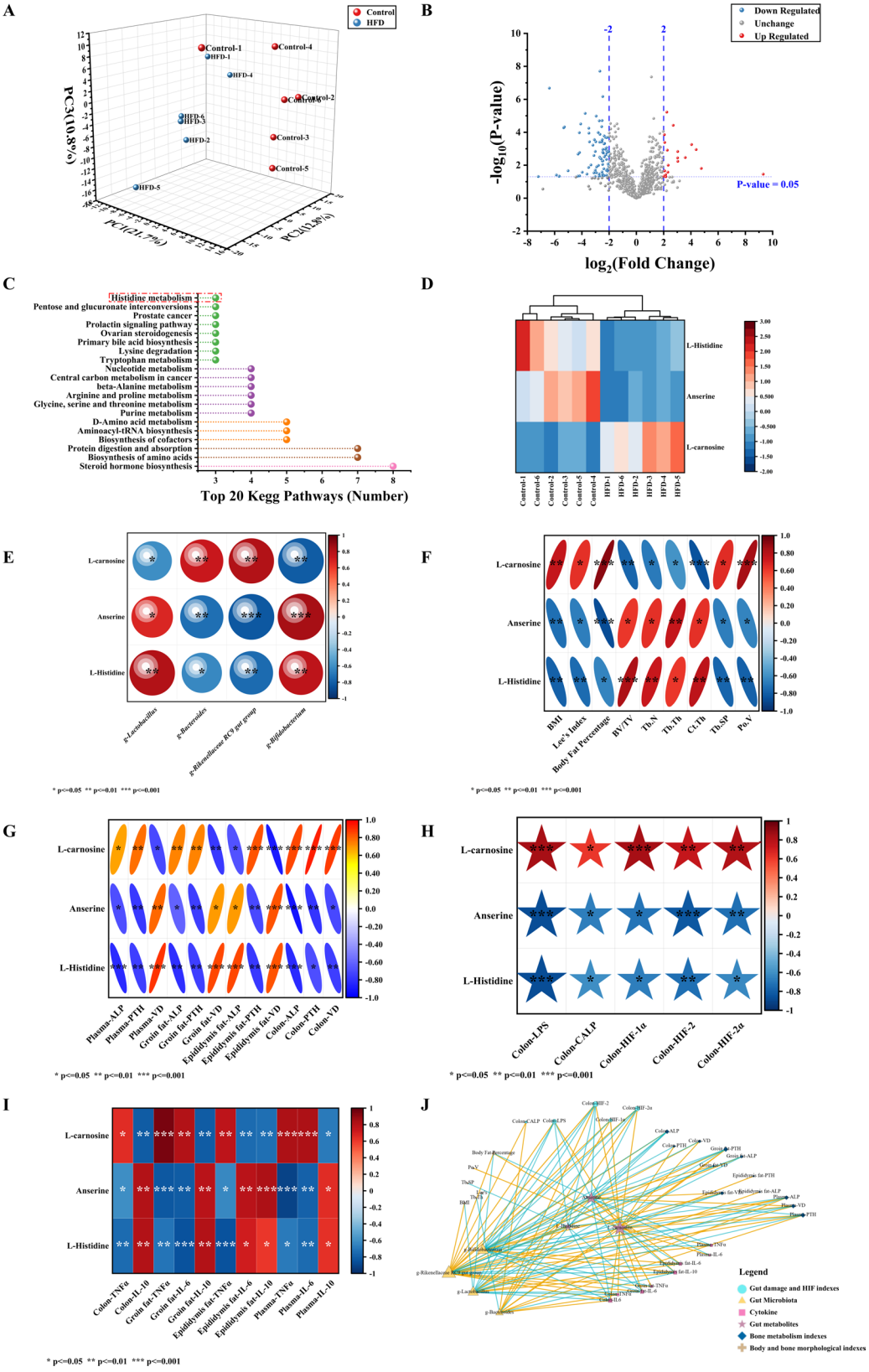

Fig. 7 (See legend on next page.)

(See figure on previous page.)

Fig. 7 Effects of a HFD on gut metabolism in mice under hypoxic conditions, with Spearman correlation analysis and network visualization. ($n = 6$). Note: (**A**) PCA; (**B**) volcano plots; (**C**) enriched KEGG pathways; (**D**) differentially expressed metabolites; (**E**) Correlation analysis between the gut microbiota and metabolites; (**F**) correlation between gut metabolites and body and bone morphological indices; (**G**) correlation analysis between gut metabolites and HIF, as well as indices of gut injury; (**H**) correlation analysis between gut metabolites and bone metabolism indices; (**I**) correlation analysis between gut metabolites and cytokines; (**J**) correlation network diagram. In Fig. 7J, the node size reflects the connectivity of each substance, defined as the number of other substances that are significantly correlated with it. Higher connectivity is represented by larger node sizes. Additionally, the thickness of the lines between nodes represents the absolute value of the correlation coefficient; a thicker line indicates a stronger correlation

methionine metabolism; alanine, aspartate, and glutamate metabolism; glycine, serine, and threonine metabolism; amino sugar and nucleotide Sugar and nucleotide Sugar metabolism; pentose phosphate pathway; galactose metabolism; fructose and mannose metabolism; phenylalanine, tyrosine, and tryptophan biosynthesis; histidine metabolism; valine, leucine, and isoleucine biosynthesis; pentose and glucan interconversions; arginine and proline metabolism; valine, leucine, leucine, and isoleucine metabolism; isobaline metabolism; isoleucine and proline degradation; tyrosine metabolism; tyrosine metabolism; taurine and Hypotaurine metabolism; and glycosaminoglycan degradation.

Differences in the relative abundance of the gut microbiota at the genus level

As shown in Fig. 6E, compared with those in the control group, the relative abundances of *g-Muribaculaceae* ($P < 0.001$), *g-Lactobacillus* ($P < 0.001$), *g-Dubosiella* ($P < 0.001$), and *g-Bifidobacterium* ($P < 0.01$) in the HFD group were significantly lower. Conversely, the relative abundances of the *g-Bacteroides* ($P < 0.001$) and *g-Rikenellaceae RC9 gut groups* ($P < 0.001$) increased significantly. Additionally, Spearman correlation analysis was conducted between the differential flora and KEGG-predicted functional pathways (Fig. 6F). The genera *g-Bacteroides* and *g-Rikenellaceae RC9 gut* groups presented positive correlations with insulin resistance, particularly in metabolic pathways such as cysteine and methionine metabolism; alanine, aspartate, and glutamate metabolism; glycine, serine, and threonine metabolism; phenylalanine, tyrosine, and tryptophan biosynthesis; histidine metabolism; valine, leucine, and isoleucine biosynthesis; arginine and proline metabolism; and valine, leucine, and isoleucine degradation. In contrast, *g-Lactobacillus* and *g-Bifidobacterium* were negatively correlated with these metabolic pathways and insulin resistance.

Effects of HFD on gut metabolism in mice under hypoxic conditions

As illustrated in Fig. 7A, principal component analysis (PCA) revealed significant differences in the composition and structure of the gut metabolites between the control and HFD groups (PC1: 21.7%, PC2: 12.8%, PC3: 10.8%). The volcano plot presented in Fig. 7B highlights the differential expression of metabolites between the two groups (P value < 0.05; log2(fold change) < -2 indicates downregulation, and log2(fold change) > 2 indicates upregulation). Specifically, 19 metabolites were upregulated, whereas 85 metabolites were downregulated. Figure 7C illustrates the top 20 enriched KEGG pathways, with histidine metabolism being consistent with the flora association pathway depicted in Fig. 6F. As shown in Fig. 7D, three differentially expressed metabolites involved in His metabolism were clustered. Compared with those in the control group, Anserine and L-Histidine were significantly downregulated, whereas L-Carnosine was significantly upregulated in the HFD group.

Spearman correlation analysis and network visualization

Correlation analysis between gut metabolites and the microbiota, as well as body and bone morphological indices

The results of the correlation analysis between the gut microbiota and metabolites are presented in Fig. 7E. L-Carnosine was significantly positively correlated with the *g-Bacteroides* and *g-Rikenellaceae RC9 gut* groups but significantly negatively correlated with the *g-Lactobacillus* and *g-Bifidobacterium gut groups*. Conversely, Anserine and L-Histidine were positively correlated with *g-Lactobacillus* and *g-Bifidobacterium* and negatively correlated with *g-Bacteroides* and *g-Rikenellaceae RC9*. As shown in Fig. 7F, anserine and L-histidine were significantly positively correlated with BS/TV, Tb.N, Tb.Th, and Ct.Th, whereas they were significantly negatively correlated with BMI, Lee's index, body fat percentage, Tb.SP, and Po.V. In contrast, L-carnitine was positively correlated with BMI, Lee's index, body fat percentage, Tb.SP, and Po.V. and negatively correlated with BS/TV, Tb.N, Tb.Th, and Ct.Th.

Correlation analysis between gut metabolites and HIF, gut injury, and bone metabolism indices

The results of the correlation analysis between the gut metabolites and the HIF and gut injury indices are presented in Fig. 7G. Specifically, Anserine and L-Histidine were significantly negatively correlated with Colon-LPS, Colon-CALP, Colon-HIF-1α, and Colon-HIF-2α, whereas L-Carnosine was positively correlated with these parameters. Furthermore, the correlation analysis between gut metabolites and bone metabolism indices is illustrated in Fig. 7H. Anserine and L-histidine were significantly positively correlated with plasma-VD, groin fat-VD, epidermis fat-ALP, and epidermis fat-VD,

whereas they were significantly negatively correlated with plasma-ALP, plasma-PTH, groin fat-ALP, groin fat-PTH, epidermis fat-PTH, Colon-ALP, Colon-PTH, and Colon-VD. Conversely, L-carnosine was significantly negatively correlated with plasma-VD, groin fat-VD, epidermis fat-ALP, and epidermis fat-VD but positively correlated with plasma-ALP, plasma-PTH, groin fat-ALP, groin fat-PTH, epidermis fat-PTH, colon-ALP, colon-PTH, and colon-VD.

Correlation analysis between gut metabolites and cytokines

The results of the correlation analysis between the gut metabolites and cytokines are shown in Fig. 7I. Anserine and L-Histidine were significantly positively correlated with Colon-IL-10, Groin fat-IL-10, Epididymis fat-IL-6, Epididymis fat-IL-10, and Plasma-IL-10. Conversely, these metabolites were significantly negatively correlated with Colon-TNFα, Groin fat-TNFα, Groin fat-IL-6, Epididymis fat-TNFα, Plasma-TNFα, and Plasma-IL-6. In contrast, L-carnosine was significantly negatively correlated with Colon-IL-10, Groin fat-IL-10, Epididymis fat-IL-6, Epididymis fat-IL-10, and Plasma-IL-10 but positively correlated with Colon-TNFα, Groin fat-TNFα, Groin fat-IL-6, Epididdidymis fat-TNFα, Plasma-TNFα, and Plasma-IL-6.

Correlation network diagram

As illustrated in Fig. 7L, the gut microbiota, including *g-Lactobacillus*, *g-Bacteroides*, *g-Rikenellaceae RC9*, and *g-Bifidobacterium*, exhibited significant correlations with gut injury, hypoxia-inducible factors, gut metabolites, and cytokines. Notably, specific gut metabolites, such as L-carnosine, anserine, and L-histidine, occupy central positions within the network. These metabolites are closely associated not only with the gut microbiome but also with bone metabolic markers and cytokines. These findings suggest that these metabolites may serve as key intermediaries in the interaction between the gut and bone tissues, participating in the regulation of bone metabolism and other critical physiological processes. Furthermore, significant associations were observed between bone metabolic indicators (ALP, PTH, and VD) and gut-related parameters (gut microbiota, gut damage indicators, and gut metabolites), as well as body and bone morphological indicators. Cytokines, including TNF-α, IL-6, and IL-10, also demonstrated significant correlations with gut-related markers and bone metabolism markers. In the correlation network diagram, the node representing the metabolite L-carnosine was notably the largest, indicating extensive connections with the gut microbiome, gut damage indicators, bone metabolism indicators, and physical and bone morphological indicators.

Discussion

In the context of global aging, osteoporosis has emerged as a prominent public health concern, significantly impacting patients' quality of life and imposing substantial medical and economic burdens [1–2]. Notably, the incidence of osteoporosis in plateau regions is markedly greater than that in lowland areas [4–6]. In plateau environments, residents often consume diets rich in protein, calories, and fat [15], which may contribute to the increased prevalence of osteoporosis. However, there is insufficient research elucidating the effects of the combination of hypoxia and high-fat diets on bone metabolism. Therefore, this study investigated the combined effects of altitude-induced hypoxia and a HFD on bone metabolism in mice, exploring the multifactorial mechanisms involved in osteoporosis through the inflammatory-bone-intestinal metabolic pathway. One of the key characteristics induced by a HFD is alterations in body weight and indices [40–41]. In this study, the mice were subjected to a HFD combined with hypoxic conditions. The results demonstrated that under identical hypoxic conditions, the body weights of the mice in the HFD group increased significantly over time compared with those of the control group. Additionally, Lee's index, BMI, and body fat percentage were markedly greater in the HFD group than in the control group. Pathological examinations further revealed that a HFD led to an enlargement of adipose tissue cells in mice. These findings indicate that a HFD successfully induced obesity in mice, which is consistent with He et al.'s observation of increased adipocyte size in HFD-fed mice [42]. The current literature also suggests that HFD-induced obesity is a significant risk factor for bone metabolic disorders [19–43]. Kim et al. reported that HFD-fed mice presented reduced trabecular volume and cortical thickness [43]. Consequently, we performed micro-CT scans and histopathological assessments of the femur, revealing that compared with the control diet, the HFD resulted in disruption of the femoral trabecular network, thinning of cortical bone, microstructural degeneration, and a significant increase in the number of osteoclasts.

In bone metabolism, ALP, PTH, and VD are among the most important markers [44–45]. Specifically, ALP is an extracellular enzyme produced by osteoblasts and serves as a key indicator of bone formation [44]. Clinical studies have demonstrated that ALP levels are linearly related to the activity of osteoblasts and preosteoblasts. The quantitative measurement and dynamic monitoring of ALP levels provide a reliable basis for the early diagnosis of bone metabolic diseases, particularly osteoporosis [46]. During the regulation of bone metabolism, calcium and phosphorus homeostasis is regulated primarily by PTH and VD [45]. Research indicates that PTH exerts dual effects on bone formation and resorption, with its

biological impact depending on dosage. At high doses, PTH increases osteoclast activity relative to osteoblast activity, leading to greater bone loss than bone formation [47]. Additionally, VD promotes calcium absorption through various tissues, regulates osteoclastogenesis, and enhances bone resorption [48]. In this study, we examined biochemical markers of bone metabolism in plasma, colon, and adipose tissue. The results indicated that a HFD induced significant increases in ALP and PTH levels in plasma, fat, and colon tissues but caused a significant decrease in VD levels. These findings align with those reported by Nirwan and Zhang et al. regarding HFD-induced osteoporosis in mice under normal conditions [18–49]. Notably, our results also suggest that a HFD can induce osteoporosis in mice under hypoxic conditions. Furthermore, a HFD led to increased expression of HIF-1α, HIF-2α, and HIF-2 in hypoxic mice. Therefore, we hypothesize that a HFD and hypoxia may have synergistic effects, potentially exacerbating bone loss in mice under hypoxic conditions. In plateau regions, the dietary patterns of Tibetan and certain ethnic minority groups are typically characterized by high-calorie and high-fat intake, whereas some Han individuals maintain a standard diet. Based on this clinical observation, we aimed to compare the effects of a normal diet versus a high-fat diet on bone metabolism in a hypoxic environment. Consequently, our study focused solely on the pathways of bone metabolic disorders induced by a HFD combined with hypoxic stimulation. The mechanisms underlying bone metabolic disorders caused by hypoxia or HFD alone, as well as the combined effects of hypoxia and HFD, remain unexplored. This represents one of the limitations of our study.

Inflammatory responses may serve as a central mechanism linking HFD consumption, hypoxia, and osteoporosis [28, 50, 51]. Since a HFD has been shown to induce osteoporosis, inflammation appears to be the primary pathway involved in this process [28]. Hypoxia also contributes to bone metabolic disorders, with inflammation likely playing a crucial role [52]. Consequently, we investigated cytokine expression in mice tissues exposed to a HFD under hypoxic conditions. Our results demonstrated that compared with the control diet, the HFD significantly increased the levels of proinflammatory factors (TNF-α and IL-6) while decreasing the levels of an anti-inflammatory factor (IL-10) in mice tissues. Moreover, a HFD exacerbated intestinal hypoxia in mice within a hypoxic environment, thereby intensifying inflammatory responses. In colonic tissue, a HFD led to epithelial cell damage, increased immune cell infiltration, alterations in the intestinal villus structure, and elevated levels of the intestinal injury markers CALP and LPS. These findings suggest that inflammatory factors exhibit significant variations both systemically and locally within the intestine. Once intestinal barrier function is compromised, harmful substances such as endotoxins can enter the bloodstream, triggering a systemic inflammatory response that affects bone tissue via the circulation. Given that inflammatory factors can directly or indirectly influence osteoblasts and osteoclasts [53–54], Shin and Johnson et al. reported that elevated TNF-α and IL-6 levels promote osteoclast differentiation and activation while inhibiting osteoblast function [55–56], which aligns with our experimental observations.

The literature has established a significant association between the gut microbiota and bone metabolism, with gut microbes influencing bone health through multiple mechanisms. The gut flora can modulate the immune system and interfere with bone metabolism [57]. Specifically, the intestinal microbiota regulates the balance between regulatory T cells (Tregs) and helper T cells 17 (Th17), maintaining Treg numbers and activity while inhibiting osteoclast overactivation. Conversely, dysbiosis of the gut microbiota may disrupt immune homeostasis, reduce Treg populations, and consequently increase osteoclastogenesis and osteoclast activity, leading to decreased bone mineral density [57–59]. Therefore, we compared the diversity of the gut microbiota in HFD-fed and control mice. Our results indicated that a HFD significantly altered the diversity and composition of the gut microbiota, characterized by a marked decrease in beneficial bacteria such as *g-Lactobacillus* and *g-Bifidobacterium* and an increase in *g-Bacteroides* and *g-Rikenellaceae RC9 in the gut*. Studies have shown that reductions in *Lactobacillus* and *Bifidobacterium* may disrupt immune balance [60–61], potentially shifting the immune response toward a pro-inflammatory state, thereby reducing Treg populations, promoting osteoclast formation and activation, and ultimately causing bone loss [57]. Moreover, increases in *Bacteroides* and the *Rikenellaceae RC9 gut group* have been associated with inflammation [62–63]. Jeon et al. reported that Bacteroides can release endotoxins, activate immune cells, and produce inflammatory mediators [64]. Inflammatory conditions may lead to the release of cytokines such as TNF-α and IL-6, which promote osteoclastogenesis and bone resorption, resulting in decreased bone density [55–57]. Additionally, inflammation may impair osteoblast function, hindering normal bone growth and repair [65]. Furthermore, long-term HFD feeding in mice results in reduced bone mass, accompanied by microbiome imbalance, increased intestinal permeability, and systemic inflammation [66]. These findings are consistent with our results demonstrating that a HFD induced an increase in inflammatory factors and the number of femoral osteoclasts in mice, resulting in bone metabolism disorders. These results suggest that HFD-induced microbiota disturbance in mice leads to alterations in the immune system. Furthermore, KEGG

functional prediction analysis of our flora revealed that multiple metabolic pathways, which are closely associated with changes in intestinal metabolites, were affected.

Therefore, we subsequently investigated changes in intestinal metabolites. Compared with those in the control group, L-histidine levels were altered in HFD-fed mice, whereas anserine was downregulated and L-carnosine was upregulated. Notably, these metabolites are involved in histidine metabolism, which is consistent with the metabolic pathways predicted by KEGG analysis of our microbiota data. Extensive studies have demonstrated a close relationship between histidine metabolism and inflammation [66], which significantly impacts bone metabolism [51]. A clinical study revealed that histidine metabolism is the most common metabolic pathway disorder in patients with low bone mineral density, leading to decreased bone mineral density and an increased risk of fractures [67]. L-Histidine, anserine, and L-carnosine all influence the bone metabolic environment through their roles in inflammatory responses [68–70]. Specifically, histamine, a product of L-histidine metabolism, acts as an inflammatory mediator [68] and can exacerbate inflammatory responses and bone destruction when it coordinates with inflammatory cytokines [71–72]. Conversely, the anti-inflammatory properties of Anserine can inhibit the release of inflammatory cytokines, thereby mitigating the adverse effects of inflammation on bone cells and maintaining normal bone cell function and tissue integrity [73]. In our findings, L-histidine serves as a precursor for histamine synthesis, and its downregulation may indicate increased histamine synthesis and subsequent inflammation. Additionally, the downregulation of Anserine suggested a diminished anti-inflammatory capacity in HFD-fed mice. Moreover, L-carnosine also has anti-inflammatory functions by inhibiting the production and release of inflammatory mediators such as IL-6 and other cytokines, thus reducing inflammation-induced damage to bone cells and supporting normal bone tissue metabolism [74–75]. Our experiment revealed that L-carnosine was upregulated in HFD-fed mice, potentially due to the inflammatory response induced by the HFD, immune system dynamic balance, and increased secretion of inflammatory factors.

Finally, Spearman correlation analysis and network visualization were employed to elucidate the multifactorial influence mechanism of a HFD on bone metabolism in mice under hypoxic conditions. These analyses revealed an intricate network in which all factors are interrelated and collectively contribute to osteoporosis development. Notably, L-carnosine occupies a central position within this network, serving as a key hub for the interaction of various factors. Under the dual stressors of hypoxia and a HFD, this network becomes imbalanced, leading to bone metabolic disorders and osteoporosis. For example, inflammatory factors can alter the composition of the gut microbiota, with microbial metabolites influencing both the inflammatory response and bone metabolism. Increased body fat modulates gut metabolism and the microbiota, which in turn impact bone tissue. This network offers a systematic perspective for understanding disease mechanisms. Future research could develop mathematical models based on these findings to simulate network dynamics under different interventions, identify core regulatory nodes, and devise multitargeted combination therapies, thereby opening new avenues for preventing and treating osteoporosis in high-altitude areas and obesity-related diseases. However, it is important to acknowledge that this study has certain limitations, particularly regarding the unverified antiosteoporotic effects of L-carnosine. Nonetheless, existing studies have demonstrated in animal models [76–77] that the supplementation of a HFD with L-carnosine significantly reduces inflammatory factor levels and inhibits the activation of inflammation-related signaling pathways (e.g., the NF-κB pathway), thereby alleviating high-fat diet-induced inflammatory responses [77]. Therefore, we hypothesize that L-carnosine exerts its antiosteoporotic function by modulating the inflammatory response, a hypothesis that will be explored in our follow-up research. In summary, this study for the first time revealed the complex mechanisms by which hypoxia, a typical factor in high-altitude environments, and HFD jointly induce osteoporosis in a mice model. The mechanisms primarily involve a vicious cycle formed through the imbalance of the metabolism-microbiome-inflammation axis (HFD induces obesity and bone metabolic imbalance), gut-bone cross-organ communication (HFD causes gut barrier damage, microbiota dysregulation, and histidine metabolic abnormalities, triggering gut-derived inflammation that affects bone tissue via the bloodstream), and the hub role of metabolites (carnosine serves as a key node in the inflammatory network, and its upregulation may represent a compensatory anti-inflammatory mechanism in the body). Different from previous studies that isolatedly explored the effects of hypoxia or HFD on bone metabolism, this study breaks through the traditional single-etiology framework and proposes a four-dimensional regulatory model of "hypoxia-HFD-microbiota-bone", revealing that HFD induces gut microbiota dysregulation and bone metabolic disorders in mice under hypoxic conditions. However, the study has limitations such as the lack of single-factor control groups, unvalidated anti-osteoporotic function of carnosine, and absence of microbial transplantation experiments. Future research may analyze the pathway roles through gene-knockout mice, conduct probiotic or metabolite intervention experiments, and validate the correlation between microbiota markers and bone mineral density

in high-altitude populations, providing a three-dimensional intervention perspective and new paradigm for the mechanism research and prevention of osteoporosis related to high-altitude environments and obesity.

Conclusion

In the context of global aging, osteoporosis has emerged as a significant public health concern, particularly in plateau regions where its incidence is notably high. This study investigated the combined effects of a HFD and hypoxia on bone metabolism in mice within a plateau environment, elucidating the underlying mechanisms through comprehensive multi-index detection and analysis. These findings indicate that a HFD induces obesity in mice under hypoxic conditions, leading to structural bone damage and alterations in bone metabolism markers (ALP and PTH increase, and VD decreases). These changes may be exacerbated by elevated HIF expression, which contributes to bone loss in hypoxic environments. Additionally, a HFD intensifies multitissue inflammation in hypoxic mice, characterized by increased levels of pro-inflammatory factors, decreased levels of anti-inflammatory factors, and systemic inflammation resulting from intestinal damage, which further compromises bone tissue integrity. Moreover, a HFD alters the diversity of the gut microbiota, with beneficial bacteria decreasing and harmful bacteria increasing. In the KEGG pathway analysis and metabolomic studies, histidine metabolism was identified as a key metabolic pathway, with down-regulation of L-histidine and anserine and upregulation of L-carnosine. These metabolites are associated with inflammation and bone metabolism. Subsequent Spearman correlation analysis revealed an interaction network among all factors, identifying L-carnosine as a critical node. While this study provides a comprehensive analysis of the mechanisms involved, the antiosteoporotic effects of L-carnosine require further verification. Future research will aim to provide strategies for disease prevention and treatment.

Abbreviations

HFD	High-fat diet
BMI	Body mass index
WHO	World Health Organization
OCR	Oxygen consumption rate
HIF	Hypoxia-inducible factor
HIF-1α	Hypoxia-inducible factor 1 subunit alpha
RANKL	Receptor activator of nuclear factor-κ B ligand
OPG	Osteoprotegerin
Dkk-1	Dickkopf-related protein 1
TNF	Tumor necrosis factor
IL-1	Interleukin-1
IL-6	Interleukin-6
IL-17	Interleukin-17
NF-κB	Nuclear factor kappa-B
PHD	Prolyl hydroxylase
IKKβ	Inhibitory kappa B kinase beta
IKK	Inhibitor of NF-κB
CNS	Central nervous system
KM	Kunming
HE	Hematoxylin and eosin
TV	Tissue volume
BV/TV	Bone volume fraction
BS/TV	Bone surface area-to-tissue volume ratio
Tb.Sp	Trabecular separation
Tb.Th	Trabecular thickness
Tb.N	Trabecular number
Tt.Ar	Total cortical bone area
Ct.Th	Cortical bone thickness
BV	Total void volume

Author contributions

All the authors materially participated in the research and article preparation. The roles of all the authors are as follows: Yajun Qiao, Huimin Zheng and Ruiying Cheng: Writing-Original Draft, Drawing. Juan Guo, Li Ji, Zhibin Liu, Lixin Wei: Writing-Review & Editing. Zhongshu Shan, Hongtao Bi: Project administration and funding acquisition.

Funding

This work was supported by the Natural Science Foundation of China (Grant No. 82171863), the Innovation Platform Program of Qinghai Province (2020-ZJ-T08), and the Tianfu Emei Project of Sichuan Province.

Data availability

The gut microbiota raw reads were deposited into the NCBI Sequence Read Archive (SRA) database (https://www.ncbi.nlm.nih.gov/search/all/?term=PRJNA1240217).

Declarations

Ethics statement

All animal experiments complied with the ARRIVE guidelines for reporting in vivo experiments and were conducted in strict accordance with the National Institutes of Health Guidelines for the Care and Use of Laboratory Animals (NIH Publication No. 8023, revised 1978). The animal experiment protocol was approved by the Animal Ethics Committee of the Northwest Plateau Biology Institute, Chinese Academy of Sciences (License number: NWIPB20171106-01).

Consent for publication

Not applicable.

Competing interests

The authors declare no competing interests.

Received: 1 April 2025 / Accepted: 5 May 2025
Published online: 16 May 2025

References

1. Sözen T, Özışık L, Başaran NÇ. An overview and management of osteoporosis. Eur J Rheumatol. 2017;4(1):46–56. https://doi.org/10.5152/eurjrheum.
2. Reginster JY, Burlet N. Osteoporosis: a still increasing prevalence. Bone. 2006;38(2 Suppl 1):S4–9. https://doi.org/10.1016/j.bone.2005.11.024.
3. Rashki Kemmak A, Rezapour A, Jahangiri R, Nikjoo S, Farabi H, Soleimanpour S. Economic burden of osteoporosis in the world: A systematic review. Med J Islam Repub Iran. 2020;34:154. https://doi.org/10.34171/mjiri.34.154.
4. Basu M, Malhotra AS, Pal K, Kumar R, Bajaj R, Verma SK, Ghosh D, Sharma YK, Sawhney RC. Alterations in different indices of skeletal health after prolonged residency at high altitude. High Alt Med Biol. 2014;15(2):170–5. https://doi.org/10.1089/ham.2013.1098.
5. Babu LK, Shaw S, Ghosh D. Bone mineral metabolism and different indices of skeletal health of Ladakhi women living at high altitude. Osteoporos Sarcopenia. 2023;9(4):131–6. https://doi.org/10.1016/j.afos.2023.11.001.
6. Zhang F, Chen Y, Wang S, Shi Z, Zhong Y, Zhu S, Wangmu C, Wu Y. Impact of altitude on the development of low bone mineral density and osteoporosis in individuals aged 50 years and older: protocol for a multicentre prospective cohort study. BMJ Open. 2024;14(8):e087142. https://doi.org/10.1136/bmjopen-2024-087142.

7. Pandit P A. The physiologic basis of high-altitude diseases. Ann Intern Med. 2005;142(7):591. https://doi.org/10.7326/0003-4819-142-7-200504050-00022. author reply 592.
8. Babu LK, Ghosh D. Looking at mountains: role of sustained hypoxia in regulating bone mineral homeostasis in relation to Wnt pathway and Estrogen. Clin Rev Bone Min Metab. 2022;20(1–4):18–36. https://doi.org/10.1007/s12018-022-09283-4.
9. Utting JC, Robins SP, Brandao-Burch A, Orriss IR, Behar J, Arnett TR. Hypoxia inhibits the growth, differentiation and bone-forming capacity of rat osteoblasts. Exp Cell Res. 2006;10(10):1693–702. https://doi.org/10.1016/j.yexcr.2006.02.007.
10. Regan JN, Lim J, Shi Y, Joeng KS, Arbeit JM, Shohet RV, Long F. Up-regulation of glycolytic metabolism is required for HIF1α-driven bone formation. Proc Natl Acad Sci U S A. 2014;111(23):8673–8. https://doi.org/10.1073/pnas.1324290111.
11. Morten KJ, Badder L, Knowles HJ. Differential regulation of HIF-mediated pathways increases mitochondrial metabolism and ATP production in hypoxic osteoclasts. J Pathol. 2013;229(5):755–64. https://doi.org/10.1002/path.4159.
12. Jaakkola P, Mole DR, Tian YM, Wilson MI, Gielbert J, Gaskell SJ, von Kriegsheim A, Hebestreit HF, Mukherji M, Schofield CJ, Maxwell PH, Pugh CW, Ratcliffe PJ. Targeting of HIF-alpha to the von Hippel-Lindau ubiquitylation complex by O2-regulated Prolyl hydroxylation. Science. 2001;292(5516):468–72. https://doi.org/10.1126/science.1059796.
13. Melis RV-TS, Maes C. Hypoxia signaling in bone physiology and energy metabolism. Curr Opin Endocr Metabolic Res. 2023;32:100473. https://doi.org/10.1016/j.coemr.2023.100473.
14. Wu C, Rankin EB, Castellini L, Alcudia JF, LaGory EL, Andersen R, Rhodes SD, Wilson TL, Mohammad KS, Castillo AB, Guise TA, Schipani E, Giaccia AJ. Oxygen-sensing phds regulate bone homeostasis through the modulation of osteoprotegerin. Genes Dev. 2015;29(8):817–31. https://doi.org/10.1101/gad.255000.114.
15. Huang Y, Liu J, Tun HM, Stanton C, Chen T, El-Nezami H, Wei H, Wang M, Wu Q. Gut microbiota insights into human adaption to high-plateau diet. Imeta. 2022;1(1):e6. https://doi.org/10.1002/imt2.6.
16. Tencerova M, Figeac F, Ditzel N, Taipaleenmäki H, Nielsen TK, Kassem M. High-Fat Diet-Induced obesity promotes expansion of bone marrow adipose tissue and impairs skeletal stem cell functions in mice. J Bone Min Res. 2018;33(6):1154–65. https://doi.org/10.1002/jbmr.3408.
17. Picke AK, Sylow L, Møller LLV, Kjøbsted R, Schmidt FN, Steejn MW, Salbach-Hirsch J, Hofbauer C, Blüher M, Saalbach A, Busse B, Rauner M, Hofbauer LC. Differential effects of high-fat diet and exercise training on bone and energy metabolism. Bone. 2018;116:120–34. 10.1016/j. bone.2018.07.015.
18. Zhang Z, Zhang Z, Pei L, Zhang X, Li B, Meng Y, Zhou X. How high-fat diet affects bone in mice: A systematic review and meta-analysis. Obes Rev. 2022;23(10):e13493. https://doi.org/10.1111/obr.13493.
19. Qiao J, Wu Y, Ren Y. The impact of a high fat diet on bones: potential mechanisms. Food Funct. 2021;12(3):963–75. https://doi.org/10.1039/d0fo02664f.
20. Huang JV, Schooling CM. Inflammation and bone mineral density: A Mendelian randomization study. Sci Rep. 2017;7(1):8666. https://doi.org/10.1038/s41598-017-09080-w.
21. Redlich K, Smolen JS. Inflammatory bone loss: pathogenesis and therapeutic intervention. Nat Rev Drug Discov. 2012;11(3):234–50. https://doi.org/10.1038/nrd3669.
22. Pham K, Parikh K, Heinrich EC. Hypoxia and inflammation: insights from High-Altitude physiology. Front Physiol. 2021;12:676782. https://doi.org/10.3389/fphys.2021.676782.
23. Liu T, Zhang L, Joo D, Sun SC. NF-κB signaling in inflammation. Signal Transduct Target Ther. 2017;2:17023. https://doi.org/10.1038/sigtrans.2017.23.
24. Cummins EP, Berra E, Comerford KM, Ginouves A, Fitzgerald KT, Seeballuck F, Godson C, Nielsen JE, Moynagh P, Pouyssegur J, Taylor CT. Prolyl hydroxylase-1 negatively regulates IkappaB kinase-beta, giving insight into hypoxia-induced NFkappaB activity. Proc Natl Acad Sci U S A. 2006;103(48):18154–9. https://doi.org/10.1073/pnas.0602235103.
25. Taylor CT. Interdependent roles for hypoxia inducible factor and nuclear factor-kappaB in hypoxic inflammation. J Physiol. 2008;586(17):4055–9. https://doi.org/10.1113/jphysiol.2008.157669.
26. Belaiba RS, Bonello S, Zähringer C, Schmidt S, Hess J, Kietzmann T, Görlach A. Hypoxia up-regulates hypoxia-inducible factor-1alpha transcription by involving phosphatidylinositol 3-kinase and nuclear factor kappab in pulmonary artery smooth muscle cells. Mol Biol Cell. 2007;18(12):4691–7. https://doi.org/10.1091/mbc.e07-04-0391.
27. Patrick, Uden V, Niall S, et al. Regulation of hypoxia-inducible factor-1alpha by NF-kappaB. Biochem J. 2008;412(3):477–84. https://doi.org/10.1042/BJ20080476.
28. Duan Y, Zeng L, Zheng C, Song B, Li F, Kong X, Xu K. Inflammatory links between high fat diets and diseases. Front Immunol. 2018;9:2649. https://doi.org/10.3389/fimmu.2018.02649.
29. Basson AR, Chen C, Sagl F, Trotter A, Bederman I, Gomez-Nguyen A, Sundrud MS, Ilic S, Cominelli F, Rodriguez-Palacios A. Regulation of intestinal inflammation by dietary fats. Front Immunol. 2021;11:604989. https://doi.org/10.3389/fimmu.2020.604989.
30. Ding S, Chi MM, Scull BP, Rigby R, Schwerbrock NM, Magness S, Jobin C, Lund PK. High-fat diet: bacteria interactions promote intestinal inflammation which precedes and correlates with obesity and insulin resistance in mice. PLoS ONE. 2010;5(8):e12191. https://doi.org/10.1371/journal.pone.0012191.
31. https://milehightraining.com/altitude-to-oxygen-chart/
32. Zhao P, Yang W, Xiao H, Zhang S, Gao C, Piao H, Liu L, Li S. Vitamin K2 protects mice against non-alcoholic fatty liver disease induced by high-fat diet. Sci Rep. 2024;14(1):3075. https://doi.org/10.1038/s41598-024-53644-6.
33. Rogers P, Webb GP. Estimation of body fat in normal and obese mice. Br J Nutr. 1980;43(1):83–6. https://doi.org/10.1079/bjn19800066.
34. Gargiulo S, Gramanzini M, Megna R, Greco A, Albanese S, Manfredi C, Brunetti A. Evaluation of growth patterns and body composition in C57Bl/6J mice using dual energy X-ray absorptiometry. Biomed Res Int. 2014;2014:253067. https://doi.org/10.1155/2014/253067.
35. Kim Y, Brodt MD, Tang SY, Silva MJ. MicroCT for scanning and analysis of mice bones. Methods Mol Biol. 2021;2230:169–98. https://doi.org/10.1007/978-1-0716-1028-2_11.
36. Bogoevski K, Woloszyk A, Blackwood K, Woodruff MA, Glatt V. Tissue morphology and antigenicity in mice and rat Tibia: comparing 12 different decalcification conditions. J Histochem Cytochem. 2019;67(8):545–61. https://doi.org/10.1369/0022155419850099.
37. Nakamura T, Kawaai K, Kuroda Y, Matsuo K. Osteoclast visualization: Tartrate-resistant acid phosphatase activity staining using NewFuchsin compatible with non-aqueous mounting and tissue clearing. MethodsX. 2024;14:103136. https://doi.org/10.1016/j.mex.2024.103136.
38. Amato KR, Yeoman CJ, Kent A, Righini N, Carbonero F, Estrada A, Gaskins HR, Stumpf RM, Yildirim S, Torralba M, Gillis M, Wilson BA, Nelson KE, White BA, Leigh SR. Habitat degradation impacts black howler monkey (Alouatta pigra) Gastrointestinal microbiomes. ISME J. 2013;7(7):1344–53. https://doi.org/10.1038/ismej.2013.16.
39. Wang C, Tong Y, Wen Y, Cai J, Guo H, Huang L, Xu M, Feng M, Chen X, Zhang J, Wu H, Kong X, Xia Q. Hepatocellular Carcinoma-Associated protein TD26 interacts and enhances sterol regulatory Element-Binding protein 1 activity to promote tumor cell proliferation and growth. Hepatology. 2018;68(5):1833–50. https://doi.org/10.1002/hep.30030.
40. Li J, Wu H, Liu Y, Yang L. High fat diet induced obesity model using four strainsof mice: Kunming, C57BL/6, BALB/c and ICR. Exp Anim. 2020;69(3):326–35. https://doi.org/10.1538/expanim.19-0148.
41. Lang P, Hasselwander S, Li H, Xia N. Effects of different diets used in diet-induced obesity models on insulin resistance and vascular dysfunction in C57BL/6 mice. Sci Rep. 2019;9(1):19556. https://doi.org/10.1038/s41598-019-55987-x.
42. He MQ, Wang JY, Wang Y, Sui J, Zhang M, Ding X, Zhao Y, Chen ZY, Ren XX, Shi BY. High-fat diet-induced adipose tissue expansion occurs prior to insulin resistance in C57BL/6J mice. Chronic Dis Transl Med. 2020;6(3):198–207. https://doi.org/10.1016/j.cdtm.2020.06.003.
43. Kim S, Henneicke H, Cavanagh LL, Macfarlane E, Thai LJ, Foong D, Gasparini SJ, Fong-Yee C, Swarbrick MM, Seibel MJ, Zhou H. Osteoblastic glucocorticoid signaling exacerbates high-fat-diet- induced bone loss and obesity. Bone Res. 2021;9(1):40. https://doi.org/10.1038/s41413-021-00159-9.
44. Greenblatt MB, Tsai JN, Wein MN. Bone turnover markers in the diagnosis and monitoring of metabolic bone disease. Clin Chem. 2017;63(2):464–74. https://doi.org/10.1373/clinchem.2016.259085.
45. Al-Daghri NM, Yakout S, Al-Shehri E, Al-Fawaz H, Aljohani N, Al-Saleh Y. Inflammatory and bone turnover markers in relation to PTH and vitamin D status among Saudi postmenopausal women with and without osteoporosis. Int J Clin Exp Med. 2014;7(9):2812–9. PMID: 25356143.
46. Nizet A, Cavalier E, Stenvinkel P, Haarhaus M, Magnusson P. Bone alkaline phosphatase: an important biomarker in chronic kidney disease - mineral and bone disorder. Clin Chim Acta. 2020;501:198–206. https://doi.org/10.1016/j.cca.2019.11.012.

47. Datta NS, Abou-Samra AB. PTH and PTHrP signaling in osteoblasts. Cell Signal. 2009;21(8):1245–54. https://doi.org/10.1016/j.cellsig.2009.02.012.
48. Ryan JW, Anderson PH, Turner AG, Morris HA. Vitamin D activities and metabolic bone disease. Clin Chim Acta. 2013;425:148–52. https://doi.org/10.1016/j.cca.2013.07.024.
49. Nirwan N, Vohora D. Linagliptin in combination with Metformin ameliorates diabetic osteoporosis through modulating BMP-2 and sclerostin in the High-Fat diet fed C57BL/6 mice. Front Endocrinol (Lausanne). 2022;13:944323. https://doi.org/10.3389/fendo.2022.944323.
50. Eltzschig HK, Carmeliet P. Hypoxia and inflammation. N Engl J Med. 2011;364(7):656–65. https://doi.org/10.1056/NEJMra0910283.
51. Lacativa PG, Farias ML. Osteoporosis and inflammation. Arq Bras Endocrinol Metabol. 2010;54(2):123–32. https://doi.org/10.1590/s0004-27302010000200007.
52. Usategui-Martín R, Rigual R, Ruiz-Mambrilla M, Fernández-Gómez JM, Dueñas A, Pérez-Castrillón JL. Molecular mechanisms involved in Hypoxia-Induced alterations in bone remodeling. Int J Mol Sci. 2022;23(6):3233. https://doi.org/10.3390/ijms23063233.
53. Di Pompo G, Errani C, Gillies R, Mercatali L, Ibrahim T, Tamanti J, Baldini N, Avnet S. Acid-Induced inflammatory cytokines in osteoblasts: A guided path to osteolysis in bone metastasis. Front Cell Dev Biol. 2021;9:678532. https://doi.org/10.3389/fcell.2021.678532.
54. Daponte V, Henke K, Drissi H. Current perspectives on the multiple roles of osteoclasts: mechanisms of osteoclast-osteoblast communication and potential clinical implications. Elife. 2024;13:e95083. https://doi.org/10.7554/eLife.95083.
55. Shin B, Kupferman J, Schmidt E, Polleux F, Delany AM, Lee SK. Rac1 Inhibition via Srgap2 restrains inflammatory osteoclastogenesis and limits the clastokine, SLIT3. J Bone Min Res. 2020;35(4):789–800. https://doi.org/10.1002/jbmr.3945.
56. Johnson RW, McGregor NE, Brennan HJ, Crimeen-Irwin B, Poulton IJ, Martin TJ, Sims NA. Glycoprotein130 (Gp130)/interleukin-6 (IL-6) signalling in osteoclasts promotes bone formation in periosteal and trabecular bone. Bone. 2015;81:343–51. https://doi.org/10.1016/j.bone.2015.08.005.
57. Zhang J, Lu Y, Wang Y, Ren X, Han J. The impact of the intestinal Microbiome on bone health. Intractable Rare Dis Res. 2018;7(3):148–55. https://doi.org/10.5582/irdr.2018.01055.
58. Atarashi K, Tanoue T, Shima T, Imaoka A, Kuwahara T, Momose Y, Cheng G, Yamasaki S, Saito T, Ohba Y, Taniguchi T, Takeda K, Hori S, Ivanov II, Umesaki Y, Itoh K, Honda K. Induction of colonic regulatory T cells by Indigenous Clostridium species. Science. 2011;331(6015):337–41. https://doi.org/10.1126/science.1198469.
59. Charles JF, Ermann J, Aliprantis AO. The intestinal Microbiome and skeletal fitness: connecting Bugs and bones. Clin Immunol. 2015;159(2):163–9. https://doi.org/10.1016/j.clim.2015.03.019.
60. Huang R, Wu F, Zhou Q, Wei W, Yue J, Xiao B, Luo Z. Lactobacillus and intestinal diseases: mechanisms of action and clinical applications. Microbiol Res. 2022;260:127019. 10.1016/j. micres.2022.127019.
61. Henrick BM, Rodriguez L, Lakshmikanth T, Pou C, Henckel E, Arzoomand A, Olin A, Wang J, Mikes J, Tan Z, Chen Y, Ehrlich AM, Bernhardsson AK, Mugabo CH, Ambrosiani Y, Gustafsson A, Chew S, Brown HK, Prambs J, Bohlin K, Mitchell RD, Underwood MA, Smilowitz JT, German JB, Frese SA, Brodin P. Bifidobacteria-mediated immune system imprinting early in life. Cell. 2021;184(15):3884–e389811. https://doi.org/10.1016/j.cell.2021.05.030.
62. Sun L, Jia H, Li J, Yu M, Yang Y, Tian D, Zhang H, Zou Z. Cecal gut microbiota and metabolites might contribute to the severity of acute myocardial ischemia by impacting the intestinal permeability, oxidative stress, and energy metabolism. Front Microbiol. 2019;10:1745. 10.3389/ fmicb.2019.01745.
63. Gao X, Chang S, Liu S, Peng L, Xie J, Dong W, Tian Y, Sheng J. Correlations between α-Linolenic Acid-Improved multitissue homeostasis and gut microbiota in mice fed a High-Fat diet. mSystems. 2020, 5(6):e00391–20. https://doi.org/10.1128/mSystems.00391-20
64. Jeon JI, Ko SH, Kim JM. Intestinal epithelial cells exposed to Bacteroides fragilis enterotoxin regulate NF-κB activation and inflammatory responses through β-Catenin expression. Infect Immun. 2019;87(11):e00312–19. https://doi.org/10.1128/IAI.00312-19.
65. Terkawi MA, Matsumae G, Shimizu T, Takahashi D, Kadoya K, Iwasaki N. Interplay between inflammation and pathological bone resorption: insights into recent mechanisms and pathways in related diseases for future perspectives. Int J Mol Sci. 2022;23(3):1786. https://doi.org/10.3390/ijms23031786.
66. Brosnan ME, Brosnan JT. Histidine metabolism and function. J Nutr. 2020;150(Suppl 1):S2070–575. https://doi.org/10.1093/jn/nxaa079.
67. Aleidi SM, Alnehmi EA, Alshaker M, Masood A, Benabdelkamel H, Al-Ansari MM, Abdel Rahman AM. A distinctive human metabolomics alteration associated with osteopenic and osteoporotic patients. Metabolites. 2021;11(9):628. https://doi.org/10.3390/metabo11090628.
68. Thakkar MM. Histamine in the regulation of wakefulness. Sleep Med Rev. 2011;15(1):65–74. https://doi.org/10.1016/j.smrv.2010.06.004.
69. Han J, Wang Z, Lu C, Zhou J, Li Y, Ming T, Zhang Z, Wang ZJ, Su X. Correction: the gut microbiota mediates the protective effects of Anserine supplementation on hyperuricaemia and associated renal inflammation. Food Funct. 2022;13(2):1027. https://doi.org/10.1039/d1fo90120f.
70. Caruso G, Fresta CG, Fidilio A, O'Donnell F, Musso N, Lazzarino G, Grasso M, Amorini AM, Tascedda F, Bucolo C, Drago F, Tavazzi B, Lazzarino G, Lunte SM, Caraci F. Carnosine decreases PMA-Induced oxidative stress and inflammation in murine macrophages. Antioxid (Basel). 2019;8(8):281. https://doi.org/10.3390/antiox8080281.
71. Branco ACCC, Yoshikawa FSY, Pietrobon AJ, Sato MN. Role of Histamine in modulating the immune response and inflammation. Mediators Inflamm. 2018;2018(9524075). https://doi.org/10.1155/2018/9524075.
72. Biosse-Duplan M, Baroukh B, Dy M, de Vernejoul MC, Saffar JL. Histamine promotes osteoclastogenesis through the differential expression of Histamine receptors on osteoclasts and osteoblasts. Am J Pathol. 2009;174(4):1426–34. https://doi.org/10.2353/ajpath.2009.080871.
73. Zhao JM, Chen X, Cheng K, Shi Q, Peng K. Anserine and glucosamine supplementation attenuates the levels of inflammatory markers in rats with rheumatoid arthritis. AMB Express. 2020;10(1):57. https://doi.org/10.1186/s13568-020-00987-8.
74. Ponist S, Drafi F, Kuncirova V, Mihalova D, Rackova L, Danisovic L, Ondrejickova O, Tumova I, Trunova O, Fedorova T, Bauerova K. Effect of carnosine in experimental arthritis and on primary culture chondrocytes. Oxid Med Cell Longev. 2016;2016:8470589. https://doi.org/10.1155/2016/8470589.
75. Caruso G. Unveiling the hidden therapeutic potential of carnosine, a molecule with a multimodal mechanism of action: A position paper. Molecules. 2022;27(10):3303. https://doi.org/10.3390/molecules27103303.
76. Park J, Jang J, Cha SR, Baek H, Lee J, Hong SH, Lee HA, Lee TJ, Yang SR. L-carnosine attenuates Bleomycin-Induced oxidative stress via NFκB pathway in the pathogenesis of pulmonary fibrosis. Antioxid (Basel). 2022;11(12):2462. https://doi.org/10.3390/antiox11122462.
77. Rašković A, Martić N, Zaklan D, Duborija-Kovačević N, Vujčić M, Andrejić-Višnjić B, Čapo I, Mijović R, Krga M, Pavlović N, Prodanović D, Arsenović P, Horvat O. Antihyperlipidemic potential of dietary supplementation with carnosine in high-fat diet-fed rats. Eur Rev Med Pharmacol Sci. 2023;27(3):1083–94. https://doi.org/10.26355/eurrev_202302_31211.

Publisher's note